

Cone tip resistance in sand: modeling, verification, and applications

M.M. Ahmadi, P.M. Byrne, and R.G. Campanella

Abstract: A numerical modeling procedure is presented to evaluate cone tip resistance in sand. The procedure involves a moving boundary simulating cone penetration. The soil is modeled as a Mohr–Coulomb elastic–plastic material with stress-dependent parameters. The procedure is verified by comparing predicted numerical values of cone tip resistance with published experimental measurements from calibration chamber tests. The selected database consists of 59 calibration chamber tests on Ticino sand with different relative densities, overconsolidation ratios, stresses, and boundary conditions. Several applications of the modeling procedure are also presented. The computer program FLAC is used to carry out the analysis.

Key words: cone tip resistance, numerical modeling, sand, calibration chamber, Mohr–Coulomb, in situ horizontal stress.

Résumé : On présente une procédure de modélisation pour évaluer la résistance de pointe du cône dans le sable. La procédure implique une frontière mobile simulant la pénétration du cône. Le sol est modélisé comme un matériau élasto-plastique Mohr–Coulomb avec des paramètres dépendant des contraintes. La procédure est vérifiée en comparant les valeurs numériques prédites de la résistance de pointe du cône avec les mesures expérimentales publiées d'essais en chambre de calibrage. La banque de données choisie comprend 59 essais en chambre de calibrage sur le sable de Ticino avec des valeurs différentes de densités, d'OCR, de contraintes et de conditions aux frontières. On présente aussi plusieurs applications de procédures de modélisation. Le programme d'ordinateur FLAC est utilisé pour réaliser l'analyse.

Mots clés : résistance à la pointe du cône, modélisation numérique, sable, chambre de calibrage; Mohr–Coulomb, contrainte horizontale in situ.

[Traduit par la Rédaction]

Introduction

Cone penetration analysis has been the subject of research for more than three decades. Many different procedures have been suggested to tackle this boundary value problem. Bearing capacity theory was one of the first methods used to predict the cone factor in clay (e.g., Meyerhof 1961; Durgunoglu and Mitchell 1975). In the bearing capacity approach the effect of soil compressibility is neglected. To account for this shortcoming, cavity expansion theory was investigated by Vesic (1972) and Yu and Houlsby (1991) and most recently by Salgado et al. (1997) and Shuttle and Jefferies (1998). A promising approach called the strain path method was suggested by Baligh (1985), and the results of analysis of penetration in clayey material based on this approach were presented by Teh and Houlsby (1991). Among other researchers, van den Berg et al. (1996) implemented a Eulerian finite element analysis of penetration in both clay

and sand. Kioussis et al. (1988) employed an elastic–plastic large strain formulation for analysis of penetration in purely cohesive material. A one-step finite element solution of steady cone penetration in undrained clay is discussed by Yu et al. (2000). Yu and Mitchell (1998) present a comprehensive review of different methods in the analysis of cone resistance.

A numerical approach for cone penetration in sand is presented in this paper. The Mohr–Coulomb elastic–plastic model with stress-dependent parameters is used in the analysis. Model parameters include the effect of sand relative density, constant-volume friction angle, and stress state. The predicted values of tip resistance are compared with the published database of experimental measurements of penetration resistance on Ticino sand at the Italian National Power Authority Hydraulic and Structural Research Centre (ENEL–CRIS) calibration chamber in Milan, Italy. The selected database contains results of experimental measurements of

Received 25 February 2002. Accepted 5 January 2005. Published on the NRC Research Press Web site at <http://cgj.nrc.ca> on 16 August 2005.

M.M. Ahmadi.¹ Department of Civil Engineering, Sharif University of Technology, P.O. Box 11365-9313, Azadi Avenue, Tehran, Iran.

P.M. Byrne and R.G. Campanella. Department of Civil Engineering, The University of British Columbia, 2324 Main Mall, Vancouver, BC V6T 1Z4, Canada.

¹Corresponding author (e-mail: mmahmadi@sharif.edu).

penetration resistance for different sand relative densities, overconsolidation ratios (OCR), horizontal and vertical stresses, and types of calibration chamber boundary conditions.

The constitutive law used for the penetration analysis is discussed, followed by a discussion of the theoretical background for the adopted procedure. Verification of the model with experimental measurements is discussed, and numerical predictions of tip resistance are compared with other numerical procedures available in the literature. Several applications of the suggested analysis are presented. The relative importance of horizontal and vertical in situ stress on the magnitude of tip resistance is discussed. The most important soil properties affecting the cone tip resistance are presented and discussed, followed by a brief discussion of the limitations of the model.

All the numerical analyses were carried out for a standard cone, i.e., a cone tip with an area of 10 cm² and an apex angle of 60°. The finite difference based computer program FLAC (Itasca Consulting Group Inc. 1998) is used for all the analysis involved in this study.

Constitutive law

The Mohr–Coulomb elastic–plastic model was chosen for the analysis of penetration. This is a simple model that can reasonably approximate the behavior of sand. The parameters needed for the model are two elastic parameters such as bulk and shear modulus, or any other combination such as constrained modulus and Poisson's ratio. Plastic parameters used in the Mohr–Coulomb model used are friction angle and dilation angle. The two elastic parameters define the assumed elastic response below the failure envelope, and friction angle and dilation angle describe the plastic response at failure.

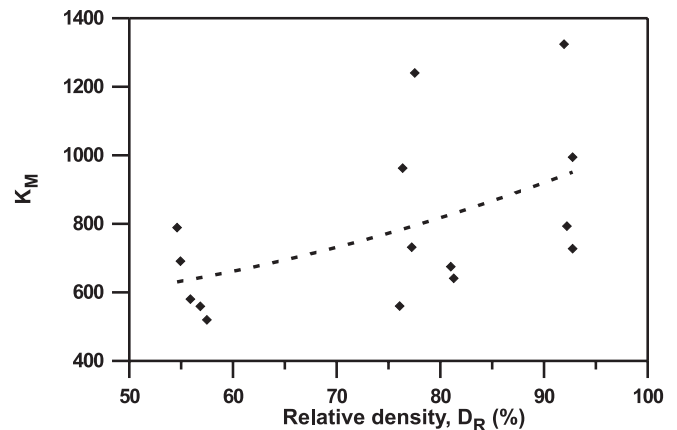
The magnitude of stresses around the cone tip during penetration becomes much greater than those far from the cone tip. Since the response of sand is stress dependent, non-intrinsic model parameters should be different in the near and far fields. Hence, in simulating the calibration chamber tests, the Mohr–Coulomb soil parameters are considered to be stress dependent.

Published experimental measurements of cone tip resistance of Ticino sand (Lunne et al. 1997) taken at the ENEL-CRIS calibration chamber are chosen as a database in this study for verification of the model. The database consists of measurements of cone tip resistance during penetration testing in the chamber. The database also consists of values of stress state, relative density, and the constrained modulus of the sand in the calibration chamber prior to penetration testing. For verification of the model, the same stress state is used in the analysis, and the values of constrained modulus for each test are used to calculate the modulus numbers needed in defining the stress-dependent elastic parameters used in the model.

The stress-dependent relation for constrained modulus, M , can be written as

$$[1] \quad M = K_M P_A (\sigma'_m / P_A)^n$$

Fig. 1. Variation of constrained modulus number (K_M) with variation of sand relative density (D_R). Data from published calibration chamber tests on Ticino sand. The broken line is the best-fit line for all data points.



where σ'_m is the mean effective stress; P_A is the atmospheric pressure, or a reference pressure, equal to 98.1 kPa; the exponent n can range from 0.2 to 0.7 and is taken to be 0.6; and K_M is the constrained modulus number that is assumed to depend only on the relative density of the sand in the calibration chamber. Based on eq. [1], and knowing constrained modulus values and horizontal and vertical stresses for each calibration chamber test, a K_M value can be calculated from the following equation:

$$[2] \quad K_M = \frac{M}{P_A \left(\frac{\sigma'_m}{P_A} \right)^n}$$

K_M depends on relative density, and the values for each calibration chamber test were computed from the data. Figure 1 shows the relation between values of K_M and relative density (D_R) for the series of normally consolidated Ticino sand tested in the calibration chamber under boundary condition type BC1. This is a boundary type in which constant horizontal (σ_h) and vertical (σ_v) stresses are applied to the chamber boundaries. Different boundary condition types are discussed later in the paper. The same value of K_M obtained for the BC1 type boundary condition is used for verification of the model for other types of boundary conditions in the chamber.

Each point in Fig. 1 represents the K_M value associated with the measurement of constrained modulus for each BC1 test with known relative density. The data show considerable scatter. The broken line in Fig. 1 is the best-fit line for all the data points considered and describes a relationship between the constrained modulus number and the sand relative density of the calibration chamber tests.

The aforementioned data for computing constrained modulus were obtained at relatively low stress levels. Soil elements close to the face of the penetrating cone will have stresses significantly higher than those in the calibration range. Equation [1] is based on tests carried out on many different sands over a wide stress range, however, and should give a

reasonable estimate of constrained modulus at high stress levels.

Poisson's ratio was chosen as the second elastic parameter and depends on shear strain or shear stress level, varying from about 0.1 at low stress levels to 0.5 at failure. In the near-field failure zone adjacent to the cone, the shear strains are controlled by the Mohr plasticity model, and the assigned Poisson's ratio has little influence. Beyond the plastic failure zone, Poisson's ratio will vary in a complex manner; to avoid introducing undue complexity, an average and constant value was chosen, as is common practice. Lambe and Whitman (1969, p.160) discuss the effect of Poisson's ratio in some detail and comment that "Fortunately, the value of Poisson's ratio has a relatively small effect upon engineering predictions."

The stress-dependent relations for elastic shear and bulk moduli (G and B) used in the Mohr–Coulomb soil model are obtained from the constrained modulus and Poisson's ratio as follows:

$$[3] \quad G = \frac{M(1 - 2\nu)}{2(1 - \nu)}$$

$$[4] \quad B = \frac{M(1 + \nu)}{3(1 - \nu)}$$

where G , B , and M are the shear, bulk, and constrained modulus, respectively; and ν is Poisson's ratio.

In this study, a constant Poisson's ratio of 0.25 was taken for the sand. Poisson's ratios of 0.20 and 0.30 were also used in some of the numerical analysis. These analyses indicate that, although Poisson's ratio does affect the predicted values of tip resistance, its influence is not significant in comparison to other factors. The reason for this insensitivity of the numerical predictions of tip resistance to Poisson's ratio is that for a specific value of constrained modulus, an increase in Poisson's ratio results in higher values of bulk modulus and lower values of shear modulus, as can be seen in eqs. [3] and [4]. It therefore appears that the opposite response of shear and bulk moduli to Poisson's ratio is balanced out in numerical predictions of tip resistance. This is in accord with Lambe and Whitman (1969).

The K_M values used in the constitutive model are given in Table 1. As shown in Table 1, the value of K_M depends only on relative density.

The data points in Fig. 1 show significant scatter, yet a clear trend of increasing K_M with an increase in relative density is observed. The values of K_M used in this study are in the range of values reported by Byrne et al. (1987). This is especially true for lower relative densities.

The Mohr–Coulomb model used also needs to be defined in terms of plastic parameters, namely friction angle and dilation angle. Baligh (1975) argues that, since the tip resistance obtained in granular material often exceeds the level of stresses ordinarily encountered in other soil mechanics applications, a realistic analysis of tip resistance in sand must therefore be based on the response of the soil at elevated stresses. This response differs from the common behavior in two important aspects: (i) the high confining stress results in a decrease in the angle of internal friction, i.e., the Mohr–Coulomb failure envelope is not straight but is actually con-

Table 1. Elastic parameters used for deformational characteristics of Ticino sand.

D_R (%)	Constrained modulus, K_M	Poisson's ratio, ν
45	585	0.25
65	690	0.25
85	870	0.25

Note: D_R , average relative density of the tested specimens at the end of consolidation.

vex; and (ii) the induced high confining stresses cause a significant decrease in volume during penetration, even for dense granular media (Baligh 1975).

To determine the shear strength parameters of Ticino sands used in the calibration chamber tests, a series of triaxial tests were carried out by ENEL–ISMES in Bergamo, Italy. Baldi et al. (1986) summarized the results of these tests in terms of the curvilinear formula proposed by Baligh (1975):

$$[5] \quad \tau_{ff} = \sigma'_{ff} \left[\tan \phi'_0 + \tan \alpha \left(\frac{1}{2.3} - \log_{10} \frac{\sigma'_{ff}}{P_A} \right) \right]$$

where τ_{ff} is the shear stress on the failure surface at failure, σ'_{ff} is the effective normal stress on the failure surface at failure, α is the angle that describes the curvature of the failure envelope, and ϕ'_0 is the secant angle of friction at $\sigma'_{ff} = 2.72P_A$.

Equation [5] can be written as

$$[6] \quad \tau_{ff} = \sigma'_{ff} [\tan \phi'_f]$$

This means that the term within the square brackets in eq. [5] can be simplified as $\tan \phi'_f$, where ϕ'_f is the effective friction angle at failure, and shows that the friction angle decreases as σ'_{ff} increases. The model therefore predicts this important behavior of sand at elevated stresses.

Other formulae could also be used to model the sand curvilinear failure envelope at high confinement stresses. Duncan et al. (1980) have proposed a model to consider the decrease in friction angle at high confinement stresses. However, since experimental measurements in the selected database are calibrated with the curvilinear formula suggested by Baligh (1975) (eq. 5), for verification of the proposed penetration model, the same model parameters are used in the analysis.

Table 2 shows published values of ϕ'_0 and α obtained from specimens at three different relative densities (Baldi et al. 1986).

The dilation angle at failure was computed from the friction angle at failure and constant-volume friction angle as follows:

$$[7] \quad \sin \psi = \sin \phi'_f - \sin \phi_{cv}$$

where ψ is the dilation angle, and ϕ_{cv} is the constant-volume friction angle for Ticino sand and is measured as 34.8° as described by Lo Presti et al. (1992). Equation [7] is based on work–energy concepts as proposed by Taylor (1948) and is described by Puebla et al. (1997).

Table 2. Plastic shear strength parameters for Ticino sand.

D_R (%)	ϕ'_0 (°)	ϕ_{cv} (°)	α (°)
45	38.2	34.8	4.2
65	40.2	34.8	6.5
85	42.9	34.8	8.1

Note: α , angle describing the curvature of the failure envelope; ϕ_{cv} , constant-volume friction angle; ϕ'_0 , secant angle of friction at $\sigma'_{ff} = 2.72 P_A$.

As can be seen from eq. [5], lower values of stress result in higher friction angles (ϕ'_f), and vice versa; and with ϕ_{cv} assumed to be a constant, higher friction angles result in higher dilation angles, as shown in eq. [7]. This means that friction angle and dilation angle are *both* stress dependent. This response of the model is in agreement with basic principles of soil mechanics. The constant-volume friction angle (ϕ_{cv}) is an intrinsic soil property, and its value is constant irrespective of the stress state.

Physics of the cone penetration mechanism

As the cone is penetrating downward in the ground, it pushes the soil particles to the side. This means that any soil particle near the axis of symmetry will be displaced horizontally. The points located on the axis of symmetry displace a horizontal distance equal to the cone radius. The soil particles will also displace a vertical distance. Figure 2 shows the pattern of deformation around a cone tip obtained from experiments (van den Berg 1994). As the figure shows, the magnitude of the vertical displacements of soil particles around the cone is not negligible.

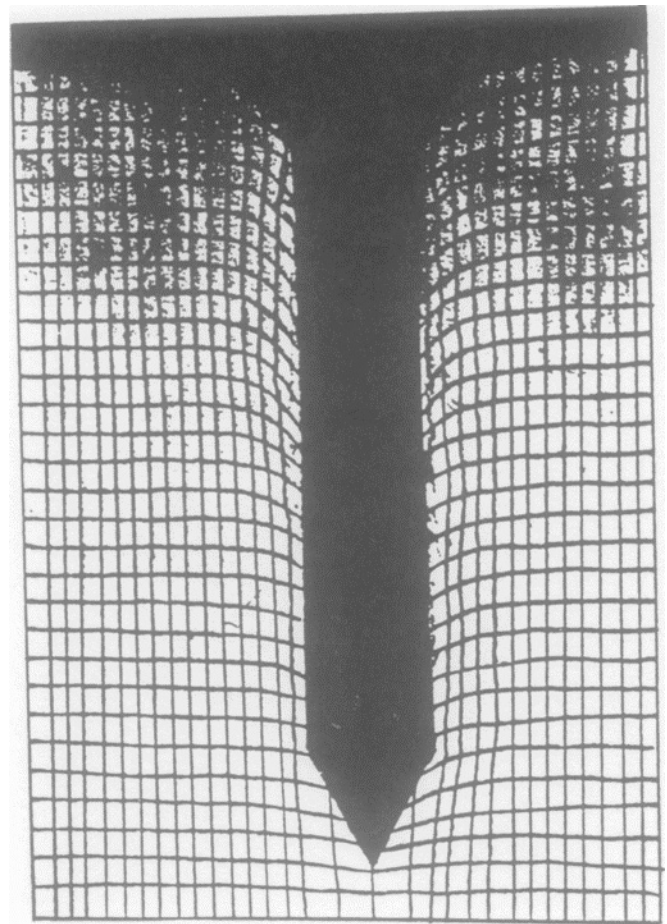
Baligh (1975) argues that the penetration process belongs, to a large extent, to the class of displacement- or strain-controlled problems where primary consideration should be given to displacements. Baligh also argues that this is in contrast to a majority of geotechnical problems that are stress controlled, and where primary consideration is given to satisfy equilibrium at the price of often neglecting strain compatibility. Based on experimental observations, Baligh argues that the deformation pattern obtained during penetration in two different soil types is more or less the same. Hence, the main criterion considered in this study is to produce a deformation pattern in the analysis that is consistent with a penetrating cone and similar to that of the experimental observations.

Numerical approach in cone penetration

The cone penetration process has been modeled by a variety of approaches. Two different approaches for cone penetration modeling have been pursued during this study. Emphasis is on the second approach, and it will be discussed at greater length later in the paper. The results presented in the paper are based on the second approach, but it is useful to briefly describe the modeling procedure and the results obtained in the first approach.

The method used in the first approach is basically a generalization of the method that has successfully been used for predicting the failure load of shallow foundations. Griffiths (1982), de Borst and Vermeer (1984), and others have pre-

Fig. 2. The deformation pattern around the cone tip obtained in experiments (after van den Berg 1994).



sented the results of their finite element analysis of cone penetration in clay. Based on a Eulerian finite element approach, van den Berg (1994) has also carried out analysis of penetration in both clay and sand. The methodology adopted in the first approach is basically similar to theirs. In this approach, the variation of stresses versus displacements at points close to the cone tip is monitored. The collapse (or failure) load is reached when the stresses remain constant with continued increase in displacement.

In the first approach the cone is placed at the mid-depth of an axisymmetric grid. The mesh close to the cone tip is more congested with elements, so the variation of response around the cone could be monitored with higher accuracy. In this model, the cone is separated from the surrounding soil by interface elements. Two types of interface elements were used, namely conical interface elements separating the conical tip from the surrounding soil, and cylindrical interface elements separating the cylinder above the cone tip from the surrounding soil.

To simulate the penetration process, the points associated with the cone in the grid are given a downward movement. This results in an increase in the stresses below and around the cone tip.

The results obtained in the first approach for penetration in both clay and sand showed that failure load could not be reached, even though the magnitude of downward cone movement was large. The cone tip resistance continued to

increase with vertical downward movements of the cone of 0.2 m and even more! No failure load could be distinguished, which means that with continued penetration the stresses do not reach a constant value. This is especially true for penetration in sand. This is not consistent with the failure load (or collapse) definition used for this approach, and it was therefore abandoned. This approach is discussed in detail by Ahmadi (2000). It is possible that a failure load could have been predicted with a cap model simulating additional compaction due to particle breakage, but this was not investigated.

A different procedure for modeling was pursued to overcome the difficulties associated with the first approach; the second approach is discussed in the following and is the main thrust of the paper.

To simulate the penetration mechanism in the second approach, the soil nodal points located along the cone path are displaced in a systematic process that starts from the top of the grid and can continue to any desired depth into the grid.

The dimensions of the numerical grid are chosen to be the same as those of the calibration chamber, which has a height of 1.5 m and a diameter of 1.2 m. Because the problem has symmetry about the vertical axis, the axisymmetric option was used for this three-dimensional problem to reduce the number of elements in the solution procedure. Throughout the paper, the figures representing the numerical grid show the axisymmetric section of the grid having a radius of 0.6 m.

Since cone penetration is basically a large-strain phenomenon and the soil under the cone tip undergoes severe deformation, the large-strain analysis implemented in the code is adopted in this approach. This means that the nodal points in the grid are continuously updated during the solution procedure.

From both the physics of the problem and the experimental evidence, points on the axis of symmetry are displaced laterally an amount equal to the radius of the cone. In the numerical analysis, however, the points located on this axis cannot accept any horizontal displacement, and an approximation must be made. Creating a cavity from zero radius is not a limitation of just FLAC. No finite element and (or) finite difference procedure could deal with such a singularity in a routine manner (J.P. Carter, personal communication, 2000).

In the proposed procedure a small vertical hole is assumed to exist at the axis of symmetry forming an inner boundary that is initially fixed in the radial direction to maintain the initial in situ stress state. This means that analysis is carried out for an axisymmetric body with a small hole down the central axis. This is discussed further at a later stage in the paper.

The progressive movement of the inner boundary simulating the penetrating cone is shown in Fig. 3. All these inner boundary points are displaced vertically and horizontally. In the present model, these points are displaced horizontally 13.4 mm (equal to three-quarters the radius of the cone). Since the radius of the hole is one-quarter the radius of the cone, this involves pushing points on the inner boundary a horizontal distance equal to three-quarters the radius of the cone. To conform to measured soil movements, vertical displacements are also imposed on these inner boundary points, and their magnitude is discussed later in the paper.

The imposed displacements are illustrated in Fig. 3 and show that during the modeling procedure the nodal point A has already been pushed away from its initial location at A' by giving a horizontal and a vertical downward displacement. Line A'-A in Fig. 3 shows the displacement vector for this point. Nodal points B, C, and D are now being pushed away from the inner boundary, and nodal point B has just been displaced sufficiently and will no longer be pushed. As the process of imposing displacement on point B is halted, point E starts to be displaced. The penetration modeling starts at the top of the grid, progresses into the grid, and can end at any desired depth in the grid, meaning that the modeling process is simulating the cone moving downward in the ground. Figures 4 and 5 show the location of the cone tip at different depths in the grid.

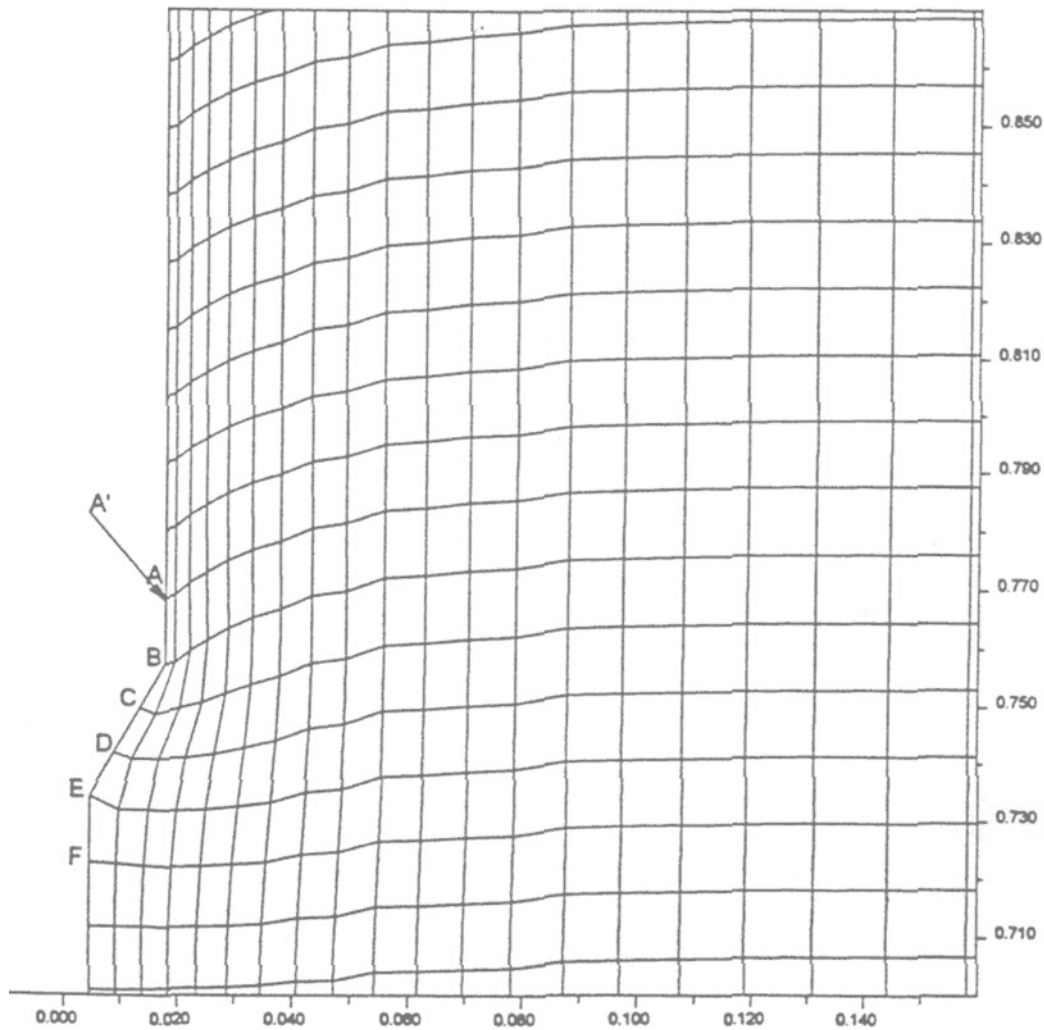
The optimum size of the artificial hole introduced into the grid depends on the solution procedure adopted. The radius of the hole should be kept small enough so that the error introduced does not significantly affect the numerical results. The inner boundary cannot be located too close to the axis of symmetry, however, because it results in a poor mesh geometry as the boundary displacement is applied. The problem is axisymmetric, and only about 5% of the cone area is ignored due to relocation of the inner boundary for a quarter of the cone radius. The error introduced is not significant.

The magnitude of the vertical displacements imposed on the nodal points located on the axis of symmetry is now discussed. In the numerical analysis, the nodal points associated with the cone face (i.e., B, C, D, and E in Fig. 3) are given a displacement vector that has two components, one in the horizontal direction and one in the vertical direction downward. Although the magnitude of the imposed horizontal component of the displacement is clear, there are no such obvious compatibility restraints for the vertical displacements around the cone. The vertical displacements are governed by slippage between the cone face and the soil. With the moving boundary approach taken, however, it was not possible to use an interface to account for this slippage. Hence an indirect approach was taken by considering ratios of vertical displacement to horizontal displacement in the range zero to unity and comparing predictions with measurements.

The analysis showed that the larger the vertical displacement component, the larger the predicted values of tip resistance. For the case when the vertical component of the imposed displacement vector is zero, i.e., no downward vertical displacement is imposed, the numerical analysis indicates that the predicted values of tip resistance are much less than those measured experimentally, and the deformation pattern around the cone does not show a vertical downward displacement similar to that observed in experiments. For the case in which the downward vertical component of the imposed displacement is large (e.g., equal to the horizontal component), the numerical analysis predicts values of tip resistances that are larger than those measured experimentally. It is concluded that a reasonable value for the vertical component of the imposed displacement should lie in the range between these two extremes.

A large number of numerical analyses were performed in which the vertical displacement was varied in this range. It was found that a vertical downward displacement equal to

Fig. 3. The deformation pattern around the cone tip obtained in the analysis. The height and radius of the grid are expressed in metres.



85% of the horizontal component of displacement imposed on the inner boundary would produce tip resistance predictions that agree best with the experimental measurements. In addition, the displacement pattern obtained in the numerical analysis is similar to that obtained with the experimental observations.

The selected vertical displacement component imposed on the inner boundary can be further verified by referring to Fig. 2, in which the vertical downward displacement around the cone is about 0.5 times the cone radius (i.e., the vertical downward displacement around the cone for this particular experiment is about 9 mm). In the analysis carried out, the vertical downward displacement is 0.85 times three-quarters of the cone radius (or about 0.6 times the cone radius). Therefore, the best-fit ratio selected is in reasonable agreement with experimental observations of van den Berg (1994) shown in Fig. 2.

The proposed procedure models the penetrating cone as a moving boundary problem in which prescribed displacements, both horizontal and vertical, are applied to an inner boundary. The inner boundary is an artifice, comprising a small cylindrical hole. Although the magnitudes of the horizontal boundary displacements are based on compatibility, no such constraint exists for the prescribed vertical boundary

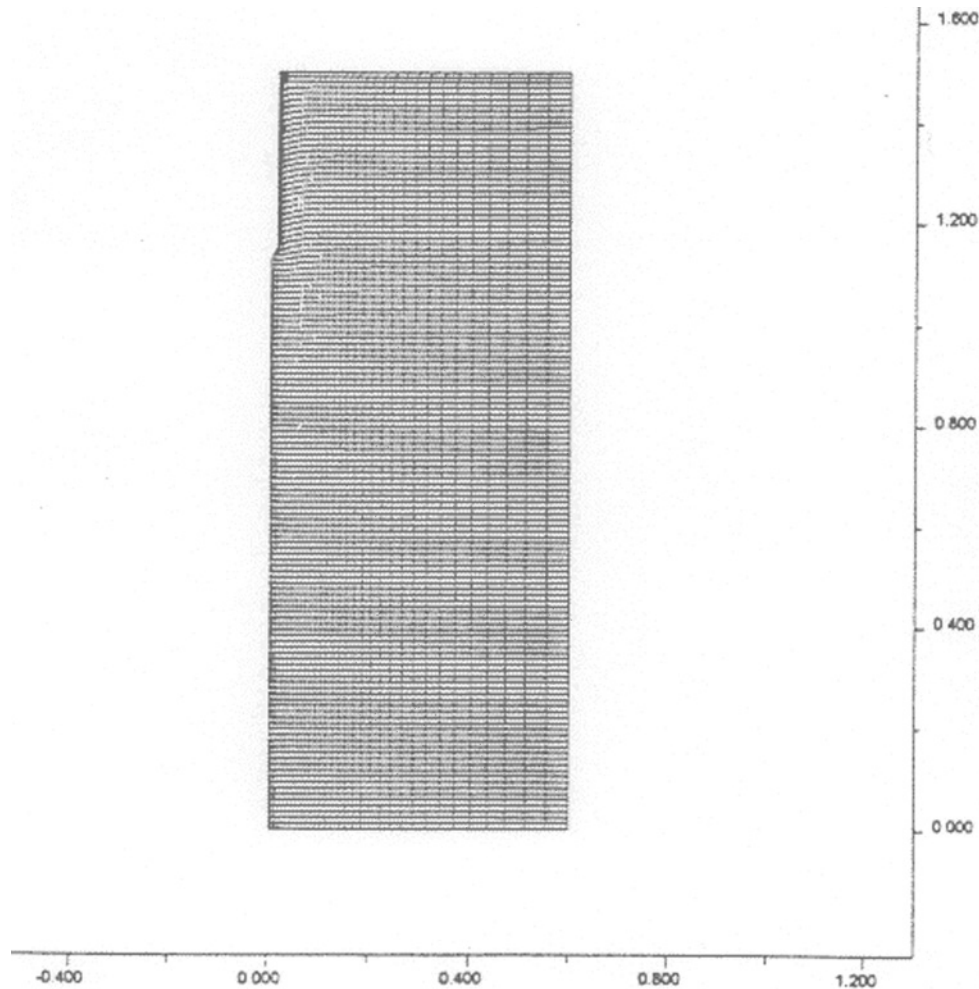
displacements, and the selected values are based on “best fit” to the observed results. An alternative approach would have been to model the moving cone itself and the interface elements between the cone and the soil. This would be difficult, however, it would remove the need for the assumption regarding prescribed vertical boundary displacements.

Calibration chamber testing

The first advanced calibration chamber where boundary stresses and strains could be measured was built in 1969 at the Country Roads Board (CRB) in Australia (Holden 1991). Currently, the chambers used in research differ in a number of ways, such as dimensions, nature and form of control of boundaries, deposition procedure, and capability to handle saturated specimens. Ghionna and Jamiolkowski (1991) provide an extensive list of most calibration chambers currently in use around the world.

The sand specimen is prepared by pluvial deposition through air. The sample is then consolidated under the desired K_0 value for the test, where K_0 is the coefficient of earth pressure at rest. This is performed by gradually apply-

Fig. 4. The location of the cone tip after a penetration of about 0.35 m. The height and radius of the grid are expressed in metres.



ing vertical stresses while restraining radial movement at the sample lateral boundary. For overconsolidated samples, the vertical stress is decreased in small increments until the desired OCR is reached.

The sand specimen is enclosed at the side and base by rubber membranes; the side membrane is sealed around an aluminum plate that forms the top rigid boundary of the specimen and transfers the thrust of the chamber piston from the sand to the lid. A hole in the centre of the lid allows the penetration of the cone into the sand specimen.

It is also possible to saturate the sand samples. Bellotti et al. (1988) argue, however, that the effect of saturation on the cone tip resistance is not significant, and penetration in sand occurs under virtually drained conditions. Therefore, dry sand has usually been used in the ENEL-CRIS calibration chamber tests.

Depending on whether stresses are kept constant or displacements are zero at the lateral and bottom sample boundaries, there are four different types of boundary conditions that can be applied during experimental testing of penetration in a calibration chamber (Ghionna and Jamiolkowski 1991). The four types of boundary conditions BC1-BC4 are listed in Table 3.

Each calibration chamber test is carried out under given values of sand relative density, horizontal stresses, and verti-

cal stresses. A large number of tests covering a wide range of densities and stresses have been carried out in the ENEL-CRIS calibration chamber. One value of cone tip resistance is obtained for each penetration test. This value corresponds to the tip resistance measured at the middle height of the chamber and is compared with the numerical value of penetration resistance obtained by the proposed modeling procedure as discussed in the next section.

Comparison of numerical results with experimental values in the calibration chamber

The numerical results for sands are compared with the experimental values obtained from penetration tests in the ENEL-CRIS calibration chamber. The test results, the properties of the sand used, and the type of boundary condition for each test are given in Lunne et al. (1997). Numerical results for all four different types of boundary condition are compared with the experimental values. However, some typical response is presented first.

Figure 6 shows how the effective friction angle decreases as a result of an increase in stress (in accordance with eq. [5]) as the cone approaches. Two locations are examined, one on the cone path and the other located at the same depth

Fig. 5. The location of the cone tip after a penetration of about 0.7 m. The height and radius of the grid are expressed in metres.

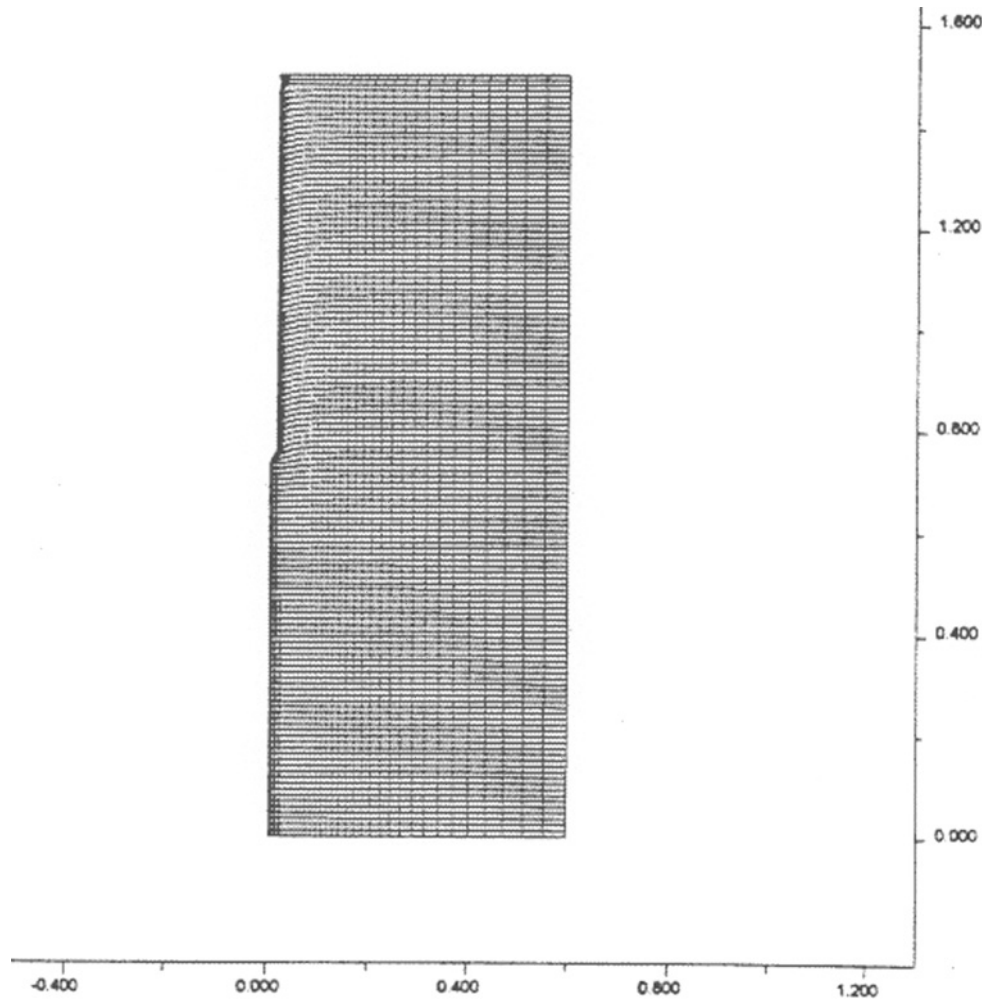


Table 3. Boundary condition types available in Italian calibration chambers.

Type of boundary condition	Lateral boundary condition		Bottom boundary condition	
	Horizontal stress, σ_h	Horizontal strain, ϵ_h	Vertical stress, σ_v	Vertical strain, ϵ_v
BC1	Constant	—	Constant	—
BC2	—	0	—	0
BC3	—	0	Constant	—
BC4	Constant	—	—	0

but farther away from the cone path, at a distance of 200 mm from the axis of symmetry. In this typical analysis, the effective vertical stress is 300 kPa and the effective horizontal stress is 150 kPa. The sand relative density is 70%. Figure 6 shows the decrease in friction angle as the cone approaches the elements. When the cone is at a vertical distance of 200 mm from the elements, the initial friction angle is close to 41° . As the cone approaches, the friction angle drops for both elements. For the element located on the cone path, however, the rate of decrease in the friction angle is higher, as expected. When the element located on the cone path comes in contact with the cone face, the friction angle drops to 34.8° , which is the value of the constant-volume friction angle (ϕ_{cv}) measured for Ticino sand as reported by

Lo Presti et al. (1992). Thus, this initially dilative element becomes so highly stressed that it no longer shows a dilative response when the face of the cone reaches it. For the element farther away from the cone path, the stresses have increased slightly, and therefore the friction angle has also decreased slightly, but not so severely as the element on the cone path. This is expected and shows that the frictional and dilative responses of the model used in this study are in agreement with basic soil mechanics theory.

Figure 7 shows a typical penetration profile obtained from the numerical analysis and presents the variation of tip resistance with the change in penetration depth of the tip. In the analysis, the cone loading is defined by specifying prescribed displacements on the inner boundary points, as dis-

Fig. 6. Typical response of the model to effective friction angle at elements located on the cone path and far from the cone path.

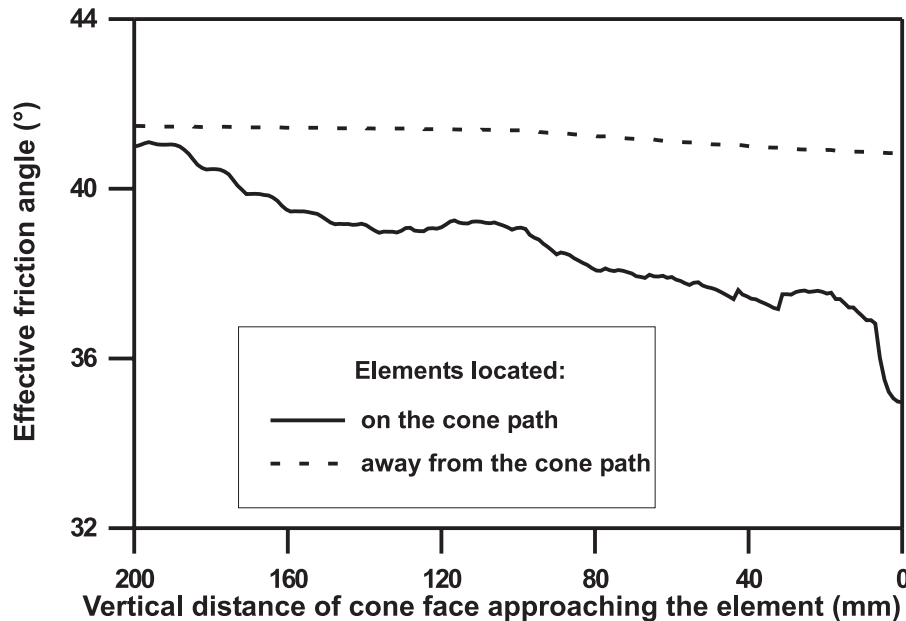
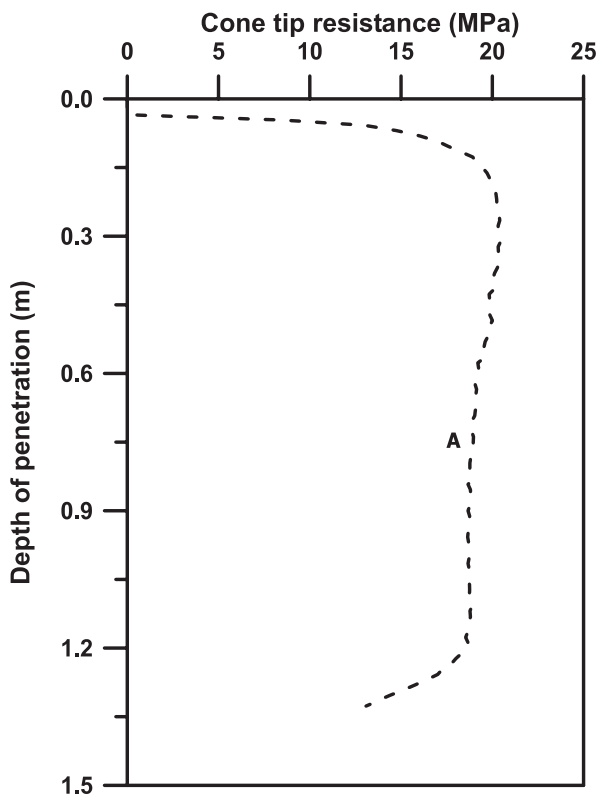


Fig. 7. Typical profile of cone tip resistance versus depth of penetration obtained in the analysis. A, mid-height of the numerical grid.



discussed in detail in previous sections in this paper. The tip force is then estimated through the integration of vertical and shearing stresses at elements associated with these points and then divided by cone area to give the tip resistance.

The height of the grid in the numerical analysis is 1.5 m, which is the same as that used for the ENEL-CRIS calibra-

tion chamber. Figure 7 shows that the cone tip resistance decreases when the cone approaches the bottom boundary. This is consistent with the experimental observations in calibration chambers and is discussed in detail by Ahmadi (2000).

The published experimental values of cone tip resistance are the values of tip resistance measured at mid-height during calibration chamber tests. To compare the results of the analysis with those from the experiments, the predicted values of cone tip resistance were also taken at mid-height of the numerical grid, i.e., point A in Fig. 7.

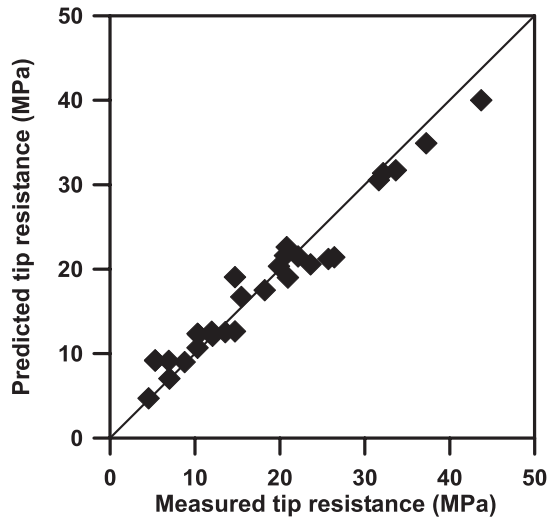
In the following sections, the results of a comparison of numerical predictions and experimental measurements for each boundary type are presented separately.

Comparison for the BC1 type boundary condition

Figure 8 shows the predicted versus experimental values of tip resistance for a series of tests with the BC1 type boundary condition for normally consolidated and overconsolidated Ticino sand. In this type of boundary condition, constant stresses are maintained in the horizontal and vertical directions in the calibration chamber. These stresses are equal to the stresses after completion of K_0 consolidation. For these tests, the relative density ranged from 53.2% to 92.8%, and the vertical stress in the chamber ranged from 61.8 to 715.1 kPa. The initial K_0 values were in the range 0.370–1.296, and the OCR values ranged from 1.00 for normally consolidated sand to 14.67 for overconsolidated sand. The points in Fig. 8 are close to the line with a slope of 45°, indicating that the predicted values obtained from numerical analysis are in agreement with the experimental values obtained in calibration chamber testing.

It is also noted that the numerical procedure systematically underpredicts the tip resistance values greater than 35 MPa. These points correspond to experiments in which confinement stresses were high. It may be possible to improve the underprediction by fine adjustment of the soil parameters used in the model. Nevertheless, Fig. 8 shows that the agreement between predicted and measured values of

Fig. 8. Agreement of predicted and measured tip resistance for BC1 type boundary condition. Relative density = 53.2%–92.8%; vertical stress = 61.8–715.1 kPa; OCR = 1.00–14.67; $K_0 = 0.370$ –1.296.



cone tip resistance is very good. The error introduced between the predicted and measured values is not more than 15% for these series of tests with the BC1 type boundary condition.

Comparison for the BC3 type boundary condition

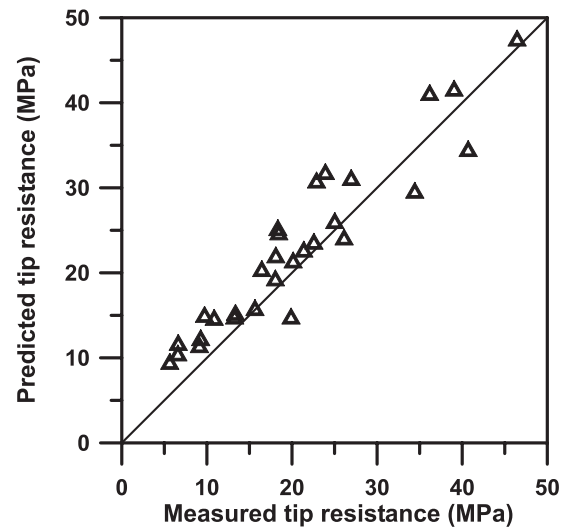
In the BC3 type of boundary condition, a constant stress is imposed at the bottom boundary during penetration testing while the displacement of the lateral boundary is kept zero. This type of test is also frequently performed in calibration chamber testing. For these series of tests, the relative density ranged from 40.2% to 94.4%, and the vertical stress in the chamber ranged from 62.8 to 716.1 kPa. The OCR ranges from 1.0 for normally consolidated sand to as high as 14.4 for overconsolidated sand. The initial K_0 value ranged from 0.39 to 1.36.

Figure 9 shows the comparison between experimental and numerical results. Most of the points are slightly above the 45° line, which means that the present model overpredicts the test results to some extent. Generally speaking, however, the difference between the test results and the numerical values is not more than 30%. In his numerical modeling of cone penetration, Salgado (1993) also reports an overprediction for BC2 and BC3 type boundary conditions. Salgado et al. (1998) associated this overprediction with experimental difficulties in achieving perfect BC3 conditions and argued that it is probably not possible to maintain (in a flexible wall calibration chamber) a radial displacement equal to zero everywhere at the sample boundary; because of this compliance at the sample boundaries, the resulting experimental values of penetration resistance are smaller than those predicted by numerical analysis.

Comparison for the BC4 type boundary condition

In the BC4 type of boundary condition, a constant stress is applied at the radial boundary while the bottom boundary is restrained, i.e., the vertical displacement at the bottom boundary is kept zero during the testing procedure. Only one

Fig. 9. Comparison between predicted and measured tip resistance for BC3 type boundary condition. Relative density = 46.2%–94.4%; vertical stress = 62.8–716.1 kPa; OCR = 1.00–14.41; $K_0 = 0.390$ –1.356.



test, test 148, was performed with the aforementioned boundary condition at the ENEL–CRIS calibration chamber with Ticino sand. For this test, the measured value of tip resistance was 25.9 MPa, and the predicted tip resistance is 26.2 MPa. The difference between measured and predicted tip resistance is 1.2%, showing very good agreement.

Comparison for the BC2 type boundary condition

In the BC2 type of boundary condition, displacement at all the boundaries (radial and bottom) is kept at zero during testing. Test 150 is the only test in the selected database that is performed with this type of boundary condition. The measured tip resistance is 29.0 MPa, and the predicted tip resistance is 37.0 MPa. For this test the numerical analysis overpredicts the measured value by 25%. This trend was also seen in BC3 type boundary condition tests in which numerical predictions were generally higher than the measured values. This again suggests that for these two types of boundary conditions (BC2 and BC3) the chamber walls were not completely restrained. The inevitable compliance introduced during testing has resulted in a decrease in the measured values of tip resistance.

To support this point further, a numerical analysis was performed for this test with the distinction that the boundary conditions were chosen to be stress controlled, i.e., boundary condition type BC1 was used instead of type BC2. For this case, the numerical analysis resulted in a tip resistance of 24.8 MPa. The measured tip resistance (29.0 MPa) lies between the two numerical values obtained under two extreme boundary conditions (tip resistance of 37.0 MPa for BC2 and 24.8 MPa for BC1). This is an indication that for BC2 and BC3 type boundary conditions there has been some compliance in the calibration chamber walls during the testing procedure.

Summary of all data

Figure 10 is a plot of all the data points for the four different boundary conditions and basically summarizes the gen-

eral behavior of the proposed model. The total number of data points shown in Fig. 10 is 59. Most of the points plot close to the 45° line, indicating that the model can predict the experimental values of calibration chamber tests reasonably well. The error band for the majority of the data points is about ±25%.

Comparison with other numerical procedures

In the preceding sections the numerical results obtained based on the proposed model were compared with experimental measurements of tip resistance. In this section, the numerical predictions of tip resistance are also compared with other numerical procedures in the literature.

The main theme of this paper has been the analysis of penetration in sandy soil, but the procedure is also applicable to penetration in clayey soil. Since most previous analyses reported in the literature are for clayey soil, in this section the comparison is made for both clayey and sandy soil.

Table 4 shows the comparison between the numerical analysis of tip resistance in clay carried out by van den Berg (1994) and the modeling procedure used in this paper. The model parameters used by van den Berg for clay are as follows: Young’s elastic modulus (E) = 6000 kPa, Poisson’s ratio (ν) = 0.49, and undrained shear strength (s_u) = 20 kPa. The in situ vertical stress (σ_v) is 50 kPa, and K_0 is assumed to be 1, i.e., in situ horizontal stress (σ_h) is also taken as equal to 50 kPa. For comparison, the same values of model parameters were used in FLAC analysis. As shown in Table 4, the cone factor, defined as $N_c = (q_c - \sigma_v) / s_u$ (where q_c is the cone tip resistance), predicted in the procedure of van den Berg is 10.8. For this case, the suggested modeling procedure gives a cone factor of 11. The agreement between both studies is very good.

The comparison is also made between the finite element solution of penetration resistance in clay suggested by Kioussis et al. (1988) and the proposed model in this study (Table 5). The problem solved by Kioussis et al. was for cone penetration into a linearly elastic, purely cohesive material. They also assume that the interface friction between the soil and penetrometer is negligible.

For the numerical analysis solved by Kioussis et al. (1988), the initial state of stress of the soil was assumed to be isotropic, with vertical and horizontal stresses equal to 100 kPa. Kioussis et al. assume a Young’s elastic modulus (E) of 30 000 kPa and a Poisson’s ratio (ν) of 0.28. The undrained shear strength (s_u) was taken to be 50 kPa. The same values of initial stress, elastic properties, and undrained shear strength are used in this study. The finite element analysis of Kioussis et al. gives a cone factor of 8.5, and the proposed analysis in this paper results in a cone factor of 11.

The model is also compared with the solution of Salgado (1993) who suggested a numerical procedure based on cavity expansion theory to predict the cone tip resistance in a sandy soil. His predictions are tested for all four different types of calibration chamber boundary condition. As described by Salgado, however, his procedure overpredicts the experimental measurements for type BC2 and BC3 boundary conditions. The comparison is therefore for type BC1 and

Fig. 10. Comparison of measured and predicted values of tip resistance for all types of boundary conditions. Broken lines indicate difference between predicted and measured tip resistance (q_c) value of 25%. Relative density = 46.2%–94.4%; vertical stress = 62.8–716.1 kPa; OCR = 1.00–14.67; K_0 = 0.370–1.356.

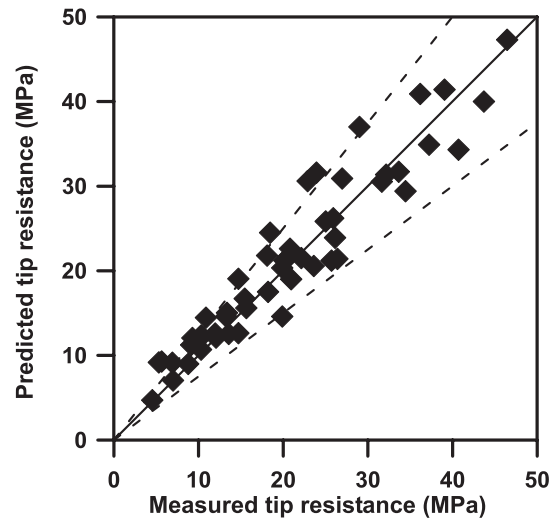


Table 4. Comparison of numerical predictions of cone tip resistance (q_c) from this study and the analysis of van den Berg (1994) for clay soil.

	Predicted q_c (kPa)	
	van den Berg	This study
Undrained shear strength, s_u (kPa)		
20	266	270

Table 5. Comparison of numerical predictions of cone tip resistance from this study with that from the solution of Kioussis et al. (1988) for clay soil.

	Predicted q_c (kPa)	
	Kioussis et al.	This study
Undrained shear strength, s_u (kPa)		
50	525	650

BC4 boundary conditions. Salgado et al. (1997) report an error band of ±30% for their numerical prediction of tip resistance for a large number of calibration chamber tests. It was not possible to compare the predictions on a one-to-one basis because the numerical prediction for each individual calibration chamber test for the Salgado et al. modeling procedure was not available. The general comparison of the proposed model in this paper with that of Salgado et al. indicates that the present model can predict the tip resistance as satisfactorily as the procedure developed by Salgado et al., with the error band obtained in this study slightly less than ±30%.

There are few independent solutions available for cone penetration test (CPT) modeling for sand in the literature with which the proposed method in this study could be compared. Therefore, the main goal in this study was to compare the numerical predictions of cone tip resistance with experi-

mental measurements. It should be recognized that the reliability of any CPT modeling procedure depends on its ability to predict the values of tip resistance obtained in controlled calibration chamber tests or field experiments.

Applications

In the previous sections the reliability of the model was investigated by comparing the predicted values of tip resistance with the measured values in the experimental chambers and with those from other numerical procedures.

In this section, several applications of the proposed model for CPT testing are presented. In the analyses to follow, the same constitutive relation that has been adopted in previous sections is used, and the model parameters are also the same.

Which in situ stress affects the tip resistance: horizontal or vertical?

There has been a debate in the literature (e.g., Baldi et al. 1986; Houlsby and Hitchman 1988; Houlsby and Wroth 1989) regarding which stress (horizontal or vertical) is more influential on the values of tip resistance obtained in cone penetration testing. Based on their experimental observations using the cone penetrometer in sand in the Oxford calibration chamber, Houlsby and Hitchman (1988) argue that, for a given density of sand, the cone tip resistance depends on the in situ effective horizontal stress, and not on the effective vertical stress. Two different series of numerical analyses were performed to investigate this issue. The sand used for both series has the same relative density, assumed to be 70%. The analyses are carried out for the BC1 type boundary condition, the height of the numerical grid is 1.5 m, and the numerical grid has a diameter of 1.2 m.

In one series of numerical analyses, the effective vertical stress is constant, and assumed to be equal to 300 kPa. The effective horizontal stress varied from 120 to 480 kPa, however, i.e., K_0 values ranged from 0.4 to 1.6. A total of five analyses were carried out in this series.

Figure 11 shows the predicted variation of tip resistance versus the variation of effective horizontal stress for this series of numerical analyses. A large increase in tip resistance with an increase in horizontal stress is shown in the figure.

The second series also consists of five numerical analyses. For these analyses, the effective horizontal stress is constant and assumed to be equal to 300 kPa. The effective vertical stress varied from 120 to 480 kPa, however. The variation of tip resistance versus effective vertical stress is shown in Fig. 12. The figure shows that this wide range of increase in the vertical stress has resulted in no appreciable increase in tip resistance. Basically, the magnitude of tip resistance remains virtually unchanged for this series of analyses in which the horizontal stress remains constant and is an indication that the tip resistance is affected by in situ horizontal stress, and not by in situ vertical stress. This is supported by the experimental observations of Baldi et al. (1986), Houlsby and Hitchman (1988), and Houlsby and Wroth (1989).

The aforementioned results also show that the OCR does not directly influence the values of cone tip resistance for sand. This means that, at a given relative density, two sandy soils with different OCRs may have the same tip resistance if their horizontal stresses are the same. This is supported by

Fig. 11. Effect of effective in situ horizontal stress on predicted tip resistance.

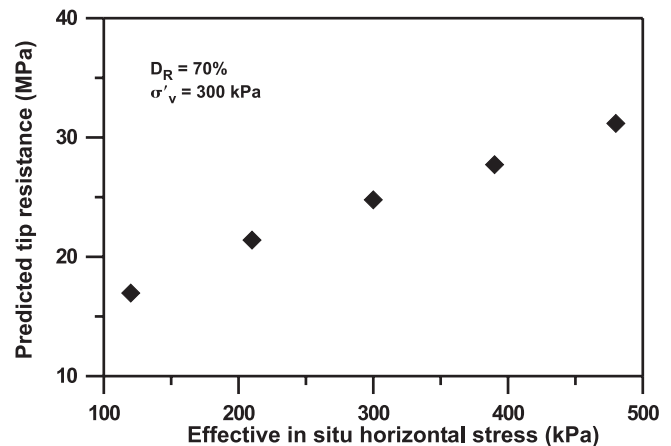
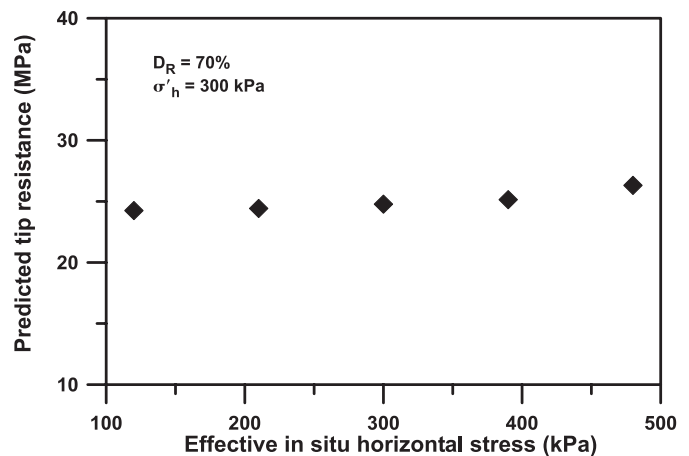


Fig. 12. Effect of effective in situ vertical stress on predicted tip resistance.



the experimental observations of Fioravante et al. (1991) and Salgado et al. (1997).

Sensitivity analysis

In real field penetration testing, the cone tip resistance is affected by a combination of soil properties (moduli, friction angle, dilation angle), and the effects of the soil properties cannot be separated. Also, in reality, soil properties are inter-related, e.g., sandy soils with higher friction angles may have higher dilatancy properties or may exhibit higher modulus values. It is instructive, however, to investigate the *separate* effect of each soil property on the cone tip resistance to see if any of the soil properties has a more important contribution to the magnitude of the cone tip resistance. A series of analyses was carried out in which only one soil property was changed and all other properties were assumed to be constant.

For these series of sensitivity analyses, the numerical grid was 1.5 m high and 4 m in diameter. The in situ effective vertical stress was taken to be 300 kPa, and K_0 was 0.5. The analyses were carried out for the BC1 type boundary condition.

Effect of soil friction angle on tip resistance

Figure 13 shows the variation of tip resistance with the variation of soil friction angle. The tip resistance increases from about 7 MPa to 9 MPa for an increase in friction angle from 32° to 44°. All other parameters, i.e., moduli and dilation angle, are considered constant. For these analyses, the constrained modulus is assumed to be 100 000 kPa. Assuming a Poisson’s ratio of 0.25, this corresponds to a bulk modulus of about 50 000 kPa and a shear modulus of about 30 000 kPa. These values are well within the range of soil moduli that can be chosen for a typical sandy soil. In this series of analyses, the dilation angle is assumed to be zero for all friction angles used in the numerical analyses. Physically, this cannot be true, i.e., the higher the friction angle, the more dilative the sand is, and these properties are interrelated as described by eq. [7]. For this investigation of the independent and separate effects of these parameters, however, only the friction angle is changed; the dilation angle and other parameters are taken as constants for all friction angles used in the analyses. This allows the relative influence of friction angle on cone tip resistance values to be quantified independently from other parameters (such as dilation angle).

Figure 13 shows that for a wide range of friction angles from 32° to 44°, which is the range that includes most sandy soils, the change in tip resistance is about ±15%. It is concluded that the effect of soil friction angle on the cone tip resistance is not large.

Effect of dilation angle on tip resistance

Figure 14 shows the variation of tip resistance with variation of the soil dilation angle while other soil properties are held constant. For this series of analyses, the friction angle is 40° and the sand constrained modulus is 100 000 kPa. The soil dilation angle is changed from -2° to 10°. This range basically covers the dilatancy characteristics of most sandy soils. A negative dilation angle in Fig. 14 corresponds to a contractive (loose) sand, and a positive dilation angle to a dilative (dense) sand. The larger dilation angles are associated with more dilative sands.

As shown in Fig. 14, the tip resistance changes from a low value of about 7.5 MPa for a soil dilation angle of -2° to a high value of about 13 MPa for a soil dilation angle of 10°. Taking a value midway between these two lower and upper values as a reference point, it can be concluded that for the range of dilation angles considered, the tip resistance is influenced by as much as 30%. Comparing Figs. 13 and 14, it can be seen that the cone tip resistance is more sensitive to the dilation characteristics of a sandy soil than to the friction angle.

Effect of modulus on tip resistance

Figure 15 shows the variation of tip resistance with variation of the soil constrained modulus. The range of constrained modulus is 25 000 – 125 000 kPa. Assuming Poisson’s ratio to be 0.25, this gives a bulk modulus range of about 12 000 – 60 000 kPa and a shear modulus range of about 8000 – 40 000 kPa. These ranges generally cover the stiffness characteristics of most sandy soils.

For all these series of analyses, the soil friction angle is assumed to be 40° and the dilation angle is assumed to be

Fig. 13. Effect of variation of friction angle on tip resistance.

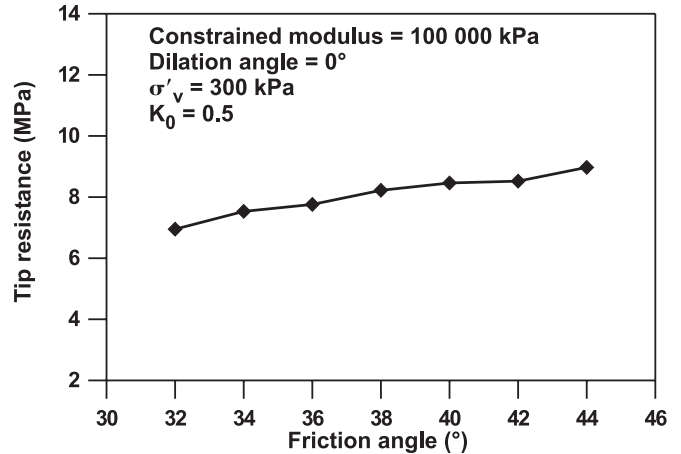
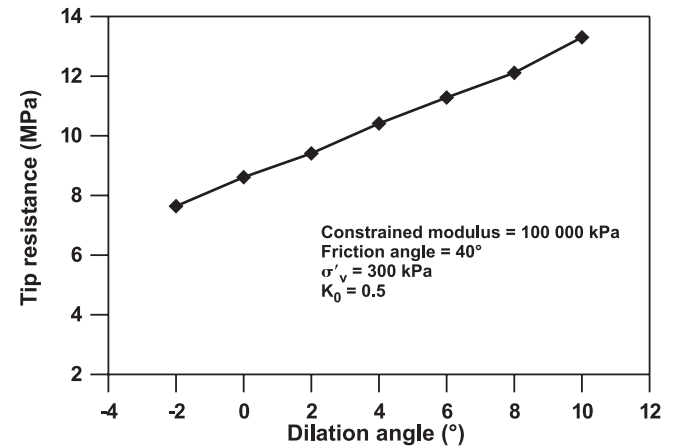


Fig. 14. Effect of variation in dilation angle on tip resistance.



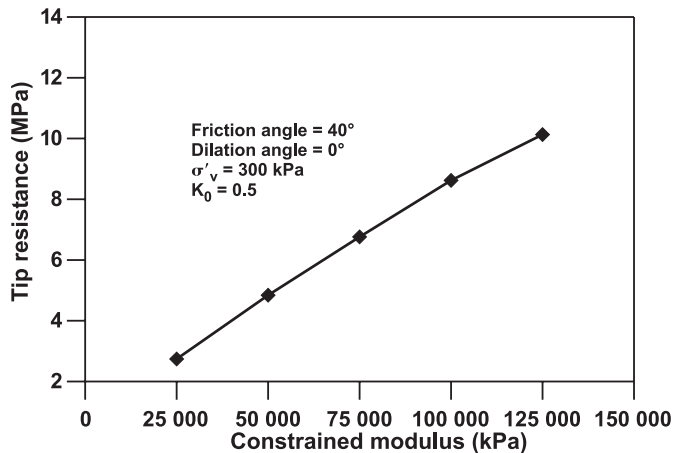
zero. For this range of modulus values, the tip resistance changes from about 3 MPa to about 10 MPa, which shows that the soil modulus has the greatest effect on tip resistance. Taking a value midway between these two values as a reference point, it is noted that the influence of the change in modulus is as much as 75% for the range of modulus considered.

Based on the aforementioned analyses, it is concluded that the soil modulus has the greatest influence on cone tip resistance. The dilatancy characteristics of sand can also change the tip resistance to a large extent; however, the sand friction angle is not a significant factor in cone tip resistance. Although cone tip resistance has commonly been related to friction angles, with higher friction angles being associated with higher tip resistances, it is likely that higher friction angles are associated with denser and stiffer sand, and it is the higher stiffness and dilation that cause the increased tip resistance.

Discussion

The modeling procedure introduced in this study is verified by comparing the numerical results of tip resistance with experimental values measured under controlled conditions in a calibration chamber. Several issues are discussed

Fig. 15. Effect of variation of constrained soil modulus on tip resistance.



in this section to clarify the weak points of the suggested modeling procedure.

Size of the selected database and its uncertainty

The database chosen for this research work is given in Lunne et al. (1997) and is mainly derived from chamber tests on Ticino sand at the ENEL–CRIS calibration chamber in Italy. It is believed that the test results are of high quality and that they can be used to derive new correlations or check new theories or interpretation methods (Lunne et al. 1997).

Nevertheless, some uncertainty should be expected for any experimental work. Sand samples may not be prepared uniformly, and the relative density of the sample may be in error by $\pm 5\%$ (Bolton 1986). The irregular penetration resistance versus depth curves resulting from possible heterogeneity of the sample will increase the degree of uncertainty as to which value to choose for the penetration resistance. Salgado (1993) reports six different types of penetration profiles versus depth obtained during tests in the calibration chamber. Based on these curves, he argues that it is not always easy to interpret with absolute certainty the value of tip resistance. As a consequence of these combined uncertainties, Salgado argues that no theoretical procedure can be expected to yield results better than $\pm 15\%$, and a procedure that predicts most experimental penetration resistance values within $\pm 30\%$ is strongly supported by experimental results.

The database selected for the verification of the modeling procedure in this paper is limited to only one sand type, i.e., Ticino sand. This is a sand that has been widely used by Italian researchers. Other researchers around the world have used other types of sand in calibration chambers. For example, Hokksund sand is widely used at the Norwegian Geotechnical Institute (NGI), and Monterey and Toyoura sands are used at the calibration chamber at the University of California at Berkeley. The modeling procedure introduced in this study should be further verified by comparison with other databases available in the literature.

Soil model used

The soil model used is a Mohr–Coulomb model with stress-dependent parameters. In this model, constrained modulus, shear modulus, bulk modulus, friction angle, and

dilation angle change with changes in the level of stress. This model is one of the simplest models that can be implemented in geotechnical problems. Nevertheless, it can capture the important characteristics of a sandy soil. The friction angle decreases as the effective mean normal stress increases. The dilation angle is related to the friction angle at failure. A drop in friction angle also results in a drop in dilation angle. As the mean normal stress increases, and the friction angle drops to the constant-volume friction angle, the dilation angle becomes zero, and dilation is completely suppressed. This model behavior is widely supported by experiments.

The model has some shortcomings, however. The sand in the field is generally anisotropic, which means that the parameters in the model should be direction dependent. The model is isotropic, however, and does not take into account such directional behavior of sand. Also, experimental observations show that sand behaves inelastically prior to failure with both elastic and plastic strain components. To preserve simplicity, this inelastic response prior to failure has not been accommodated in the model presented in this paper.

Mesh size around the cone tip

In the geometric modeling, there are eight elements associated with the cone diameter. This number of elements seems to be sufficient to result in an acceptable response. This is a region where the stress gradient is large, however, and from a theoretical standpoint it is preferred to have more elements around the cone tip.

In the FLAC analysis used, the mesh changes as displacements are prescribed, and if a finer mesh is used, the elements become ill-shaped; the program signals a “Bad Geometry” message, and the analysis is halted. FLAC does not have an automatic remeshing facility, and it is cumbersome to do this manually. This limits the capability of this study to investigate the element size effect.

Interface friction between soil and penetrometer

In the suggested modeling procedure (the second approach) presented in this paper, the soil nodal points are pushed aside to create a hole in the grid and produce a deformation pattern in the analysis similar to those observed experimentally. In this procedure, the penetrometer itself is not modeled, and hence interface elements along the penetrometer and the soil surrounding it are not included in the analysis. The present analysis has the shortcoming of giving no concrete information about the magnitude of interface frictional stresses produced during penetration along the cone face and along the sleeve. The prescribed vertical deflection at the cone boundary indirectly includes the effect of interface friction, however. A direct measure of the effect of cone roughness on interface angle or cone resistance is an important but unanswered question.

Sand in the calibration chamber versus sand in the field

The sand tested in the calibration chamber is clean, non-cemented, unaged sand. In the field, however, the sand deposit may have some amount of fines content, may be aged, and may also be cemented to some degree. Aging of sand or a light amount of cementation may significantly increase the

tip resistance. This increase may be due to an increase in strength or stiffness of the cemented material (Ghionna and Jamiolkowski 1991). From this study, increased penetration due to aging is likely largely due to increased stiffness rather than increased strength. Hence relationships developed between tip resistance and soil modulus are likely to be more reliable for field conditions than other relationships such as tip resistance versus friction angle.

The features and attributes of naturally occurring sand, such as cementation, aging, fabric, or particle size, should be reviewed more extensively in both experimental and numerical research in cone penetration testing.

Final thoughts: CPT research advanced, but ...

In the last several sections and paragraphs a model is suggested to predict the cone tip resistance, provided the soil parameters are known. The theme of the paper is as follows: "Given the soil properties, can the cone tip resistance be predicted?" In reality, what is needed in geotechnical practice is just the opposite. Given the tip resistance, is it possible to predict some soil parameters for use in analysis and design? If the cone tip resistance measurements are available, which soil parameters can be predicted, and how reliable are they? Is it possible to estimate soil properties from tip resistance alone, or is it necessary to combine tip measurements with other measurements during CPT penetration, e.g., pore pressure and seismic wave velocity, to predict reliable stress-strain parameters for soil?

Although the present study has shed some light on soil parameters that have an important contribution to the magnitude of the cone tip resistance, it does not completely respond to the needs of a geotechnical practitioner in the selection of soil parameters required for design. Research and study need to be continued until this essential aspect of site characterization is adequately addressed.

Conclusion

A numerical model has been developed for the prediction of cone tip resistance in sand and involves a simple elastic-plastic stress-strain law with two elastic parameters and two plastic parameters. The elastic parameters involve a constrained modulus that varies with stress level and Poisson's ratio that is assumed constant. The plastic parameters are the friction angle and dilation angle, and both vary with variations in soil density and stress level.

The soil domain is modeled as a collection of elements, and the cone is modeled as a prescribed moving boundary. In this way, the penetration of the cone from the ground surface to the full depth of the soil strata can be simulated. Unlike other more routine geotechnical problems that are stress controlled, the penetration problem is displacement controlled. In essence, the numerical procedure described in this paper is built on this distinct physical concept of imposing a prescribed displacement at nodal points at an inner moving boundary.

The model was calibrated and verified by comparison with cone tests carried out under controlled conditions in calibration chamber tests. The database of chamber tests used for evaluating the present model contains tests that cover a wide range of values of sand relative density, stress

state, moduli, and overconsolidation ratio (OCR). Comparisons between predicted and experimental measurements of penetration resistance for Ticino sand at the ENEL-CRIS calibration chamber were satisfactory. Generally, the error band between predicted and measured values was $\pm 25\%$.

The analyses showed that the in situ horizontal stress is a dominant factor in tip resistance, and that varying the vertical stress while keeping the in situ horizontal stress constant had virtually no effect on cone tip resistance. This is in agreement with the calibration chamber test data.

Having verified the procedure under controlled calibration chamber test conditions, the numerical results were also compared with other numerical procedures carried out for analysis of penetration in both clayey and sandy soils. The agreement between predictions of tip resistance obtained from this study and other available predictions in the literature was satisfactory.

The results of a sensitivity analysis reveal that the cone tip resistance is mostly a measure of soil modulus. Higher tip resistance is mainly due to higher soil modulus. Dilation angle is also important, with higher dilation angles giving higher tip resistances. The analyses show that tip resistance is only marginally increased by an increase in the friction angle. In practice, the friction angle is related to density, which affects stiffness and in turn can substantially increase cone tip resistance. Friction angle itself, however, does not contribute significantly to tip resistance.

The conclusions are based on the assumptions of the soil parameters and the model used. Although the model parameters are selected to be generally realistic, there may be situations where extrapolation of the results obtained in this study needs further verification.

Acknowledgment

The authors are grateful to the Natural Sciences and Engineering Research Council of Canada (NSERC) for their financial support.

References

- Ahmadi, M.M. 2000. Analysis of cone tip resistance in sand. Ph.D. thesis, The University of British Columbia, Vancouver, B.C.
- Baldi, G., Bellotti, R., Ghionna, V., Jamiolkowski, M., and Pasqualini, E. 1986. Interpretations of CPTs and CPTUs, Part II: drained penetration of sands. *In Proceedings of the 4th International Geotechnical Seminar on Field Instrumentation and In-situ Measurements*, Singapore, 25–27 November 1986. Nanyang Technological Institute, Singapore. pp. 143–156.
- Baligh, M.M. 1975. Theory of deep site static cone penetration resistance. Publication R75-56, Department of Civil Engineering, Massachusetts Institute of Technology, Cambridge, Mass.
- Baligh, M.M. 1985. Strain path method. *Journal of Geotechnical Engineering*, ASCE, **111**(GT9): 1108–1136.
- Bellotti, R., Crippa, V., Pedroni, S., and Ghionna, V.N. 1988. Saturation of sand specimen for calibration chamber tests. *In Proceedings of the 1st International Symposium on Penetration Testing (ISOPT-1)*, Orlando, Fla., 20–24 March 1988. Edited by J. DeRuiter. A.A. Balkema, Rotterdam, The Netherlands. Vol. 2, pp. 661–671.
- Bolton, M.D. 1986. The strength and dilatancy of sand. *Géotechnique*, **36**(1): 65–78.

- Byrne, P.M., Cheung, H., and Yan, L. 1987. Soil parameters for deformation analysis of sand masses. *Canadian Geotechnical Journal*, **24**: 366–376.
- de Borst, R., and Vermeer, P.A. 1984. Possibilities and limitations of finite elements for limit analysis. *Géotechnique*, **34**(2): 199–210.
- Duncan, J.M., Byrne, P.M., Wong, K.S., and Marby, P. 1980. Strength, stress–strain, and bulk modulus parameters for finite element analysis of stresses and movements in soil masses. Report UCB/GT/80-01, University of California at Berkeley, Berkeley, Calif.
- Durgunoglu, H.T., and Mitchell, J.K. 1975. Static penetration resistance of soils. I: analysis. *In Proceedings of the ASCE Specialty Conference on In-Situ Measurement of Soil Properties*, Raleigh, N.C. ASCE, New York. Vol. 1, pp. 151–171.
- Fioravante, V., Jamiolkowski, M., Tanizawa, F., and Tatsuoaka, F. 1991. Results of CPTs in Toyoura quartz sand. *In Proceedings of the 1st International Symposium on Calibration Chamber Testing (ISOCCT-1)*, Potsdam, N.Y., 28–29 June 1991. pp. 135–146.
- Ghionna, V., and Jamiolkowski, M. 1991. A critical appraisal of calibration chamber testing of sands. *In Proceedings of the 1st International Symposium on Calibration Chamber Testing (ISOCCT-1)*, Potsdam, N.Y., 28–29 June 1991. pp. 13–39.
- Griffiths, D.V. 1982. Elasto-plastic analysis of deep foundations in cohesive soil. *International Journal for Numerical and Analytical Methods in Geomechanics*, **6**: 211–218.
- Holden, J.C. 1991. History of the first six CRB calibration chambers. *In Proceeding of the 1st International Symposium on Calibration Chamber Testing (ISOCCT-1)*, Potsdam, N.Y., 28–29 June 1991. pp. 1–11.
- Houlsby, G.T., and Hitchman, R. 1988. Calibration chamber tests of a cone penetrometer in sand. *Géotechnique*, **38**(1): 39–44.
- Houlsby, G.T., and Wroth, C.P. 1989. The influence of soil stiffness and lateral stress on the results of in-situ soil tests. *In Proceedings of the 12th International Conference on Soil Mechanics and Foundation Engineering*, Rio de Janeiro, Brazil, 13–18 August 1989. A.A. Balkema, Rotterdam, The Netherlands. Vol. 1, pp. 227–232.
- Itasca Consulting Group Inc. 1998. *FLAC user manual*, version 3.4. Itasca Consulting Group Inc., Minneapolis, Minn.
- Kiousis, P.D., Voyiadjis, G.Z., and Tumay, M.T. 1988. A large strain theory and its application in the analysis of the cone penetration mechanism. *International Journal for Numerical and Analytical Methods in Geomechanics*, **12**: 45–60.
- Lambe, T.W., and Whitman, R.V. 1969. *Soil mechanics*. John Wiley & Sons, Inc., New York. 553 pp.
- Lo Presti, D.C.F., Pedroni, S., and Crippa, V. 1992. Maximum dry density of cohesionless soils by pluviation and by ASTM D 4253-83: a comparative study. *Geotechnical Testing Journal*, **15**(2): 180–189.
- Lunne, T., Robertson, P.K., and Powell, J.M. 1997. *Cone penetration testing in geotechnical practice*. Blackie Academic & Professional, London, UK.
- Meyerhof, G.G. 1961. The ultimate bearing capacity of wedge shaped foundations. *In Proceedings of the 5th International Conference on Soil Mechanics and Foundation Engineering*, Paris. Vol. 2, pp. 103–109.
- Puebla, H., Byrne, P.M., and Phillips, R. 1997. Analysis of CANLEX liquefaction embankments: prototype and centrifuge models. *Canadian Geotechnical Journal*, **34**(5): 641–657.
- Salgado, R. 1993. Analysis of penetration resistance in sand. Ph.D. thesis, Department of Civil Engineering, University of California at Berkeley, Berkeley, Calif.
- Salgado, R., Mitchell, J.K., and Jamiolkowski, M. 1997. Cavity expansion and penetration resistance in sand. *Journal of Geotechnical and Geoenvironmental Engineering, ASCE*, **123**(4): 344–354.
- Salgado, R., Mitchell, J.K., and Jamiolkowski, M. 1998. Calibration chamber size effects on penetration resistance in sand. *Journal of Geotechnical and Geoenvironmental Engineering, ASCE*, **124**(9): 878–888.
- Shuttle, D., and Jefferies, M. 1998. Dimensionless and unbiased CPT interpretation in sand. *International Journal for Numerical and Analytical Methods in Geomechanics*, **22**: 351–391.
- Taylor, D.W. 1948. *Fundamentals of soil mechanics*. John Wiley & Sons, Inc., New York.
- Teh, C.I., and Houlsby, G.T. 1991. An analytical study of the cone penetration test in clay. *Géotechnique*, **41**(1): 17–34.
- van den Berg, P. 1994. Analysis of soil penetration. Ph.D. thesis, Delft University of Technology, Delft, The Netherlands.
- van den Berg, P., de Borst, R., and Huetink, H. 1996. An Eulerian finite element model for penetration in layered soil. *International Journal for Numerical and Analytical Methods in Geomechanics*, **20**: 865–886.
- Vesic, A.S. 1972. Expansion of cavities in infinite soil mass. *Journal of the Soil Mechanics and Foundations Division, ASCE*, **98**(GT3): 265–290.
- Yu, H.S., and Houlsby, G.T. 1991. Finite cavity expansion in dilatant soil: loading analysis. *Géotechnique*, **41**(2): 173–183.
- Yu, H.S., and Mitchell, J.K. 1998. Analysis of cone resistance: review of methods. *Journal of Geotechnical and Geoenvironmental Engineering, ASCE*, **124**(2): 140–147.
- Yu, H.S., Herrmann, L.R., and Boulanger, R.W. 2000. Analysis of steady cone penetration in clay. *Journal of Geotechnical and Geoenvironmental Engineering, ASCE*, **126**(7): 594–605.

List of symbols

- B bulk modulus
- BC1 boundary condition type 1 ($\sigma_h = \text{constant}$, $\sigma_v = \text{constant}$)
- BC2 boundary condition type 2 ($\epsilon_h = 0$, $\epsilon_v = 0$)
- BC3 boundary condition type 3 ($\epsilon_h = 0$, $\sigma_v = \text{constant}$)
- BC4 boundary condition type 4 ($\epsilon_v = 0$, $\sigma_h = \text{constant}$)
- D_R relative density of the sand in the chamber before penetration and after consolidation
- E Young's elastic modulus
- G shear modulus of soil
- K_M constrained modulus number
- K_0 coefficient of earth pressure at rest or coefficient of lateral stress before penetration
- M constrained modulus
- n exponent
- N_c cone factor in clay
- OCR overconsolidation ratio
- P_A atmospheric pressure
- q_c cone tip resistance
- s_u undrained shear strength
- α angle describing the curvature of the failure envelope
- ϵ_h horizontal strain
- ϵ_v vertical strain
- ϕ_{cv} constant-volume friction angle
- ϕ'_f effective friction angle at failure
- ϕ'_0 secant angle of friction at $\sigma'_{ff} = 2.72P_A$
- ψ dilation angle

ν Poisson's ratio
 σ'_{ff} effective normal stress on the failure surface at failure
 σ'_h effective horizontal stress
 σ_h total horizontal stress

σ'_m mean effective stress
 σ_v total vertical stress
 σ'_v effective vertical stress
 τ_{ff} shear stress on the failure surface at failure